Dalton Transactions

PAPER

View Article Online
View Journal

Cite this: DOI: 10.1039/c6dt03769k

Structure models for the hydrated and dehydrated nitrate-intercalated layered double hydroxide of Li and Al†

Supreeth Nagendran, Ganga Periyasamy and P. Vishnu Kamath*

Received 28th September 2016,
Accepted 12th October 2016

DOI: 10.1039/c6dt03769k

www.rsc.org/dalton

Imbibition of $LiNO_3$ into gibbsite results in the formation of a single phase layered double hydroxide of the composition $LiAl_2(OH)_6(NO_3)\cdot 1.2H_2O$. This phase undergoes reversible dehydration along with the compression of the basal spacing accompanied by the reorientation of the nitrate in the interlayer gallery. The hydrated phase is a solid solution of two lattices: (i) a hexagonal lattice defining the ordering of atoms within the metal hydroxide layer, and (ii) a lattice of orthorhombic symmetry defining the ordering of atoms within the interlayer. DFT calculations of the hydration behaviour show that there is no registry between the two sublattices. In the dehydrated phase, the nitrate ion is intercalated with its molecular plane parallel to the metal hydroxide layer and the crystal adopts a structure of hexagonal symmetry.

Introduction

The layered double hydroxides (LDHs) of Li^+ and Al^{3+} having the general formula $[LiAl_2(OH)_6]X\cdot mH_2O$ (X = Cl^-, Br^-, NO_3^-; m = 2–3) are generally obtained by the "imbibition" of Li^+ ions into the octahedral vacancies of $Al(OH)_3$.[1] $Al(OH)_3$ adopts a structure isotypic with $Mg(OH)_2$, wherein three Mg^{2+} ions are replaced by two Al^{3+} ions, leaving one cation vacancy. The "molecular" formula of $Al(OH)_3$ is more accurately represented as $[Al_2\square(OH)_6]$ (□: octahedral vacancy).[2] The imbibition of Li^+ ions in the metal hydroxide layer imparts a positive charge to the layer. The composition of the metal hydroxide layer is $[LiAl_2(OH)_6]^+$. The layer charge is compensated by the incorporation of anions in the interlayer galleries. As the synthesis of metal hydroxides is usually carried out in aqueous medium, water molecules are also included in the interlayer galleries in the form of the hydration sphere of the anions.[3] For the purpose of brevity, we refer to the LDH formula by the symbol [Li–Al–X] (X = anion).

While the structure of the metal hydroxide layers and the manner in which they are stacked are well known,[4] there is relatively little understanding of the packing of atoms in the interlayer galleries. Several factors affect the manner in which the atoms are packed in the interlayer: (i) orientation of the anions relative to the stacking direction, (ii) degree of hydration, which affects the number density of atoms in the interlayer galleries, (iii) the interplay between the coulombic and hydrogen bonding interactions between the metal hydroxide layer and the interlayer, and (iv) similar competing forces operating between various intercalated moieties. The situation is further complicated when (i) the intercalated moieties comprise light atoms, and (ii) the intercalated water molecules are exchanged with water molecules in the ambient. This last factor results in a range of temperature-driven and humidity-driven structural transitions in different LDH systems.[5]

One of the early attempts to investigate the structure of the gibbsite-derived [Li–Al–X] (X = Cl^-, Br^-, NO_3^-) LDHs was made by Besserguenev and coworkers.[6] They refined the structures of the hydrated and dehydrated phases of the [Li–Al–Cl] LDH using both X-ray and neutron diffraction data. The Cl^- ion exhibits extensive positional disorder in the hydrated phase, but gets ordered upon dehydration. They also refined the structures of the dehydrated phases of [Li–Al–X] (X = Br^-, NO_3^-) LDHs, as they were more ordered compared to their hydrated analogues.

In later work[7] it was shown that the [Li–Al–Br] LDH crystallizes in two different structures depending upon ambient humidity. The two structures differ solely in the manner in which the atoms are packed in the interlayer gallery. At a low relative humidity (RH ~ 29%), the Br^- ion occupies a site proximal to Li^+, which is the seat of the positive charge of the metal hydroxide layer. At high values of the relative humidity (RH > 79%), the water molecules occupy sites proximal to Li^+ and provide a distant hydration sphere to Li^+. The Br^- ions move to a different site. This humidity driven structural transition is not only reversible, but also takes place without any change in the basal spacing.

Department of Chemistry, Central College, Bangalore University, Bangalore 560 001, India. E-mail: vishnukamath8@hotmail.com

†Electronic supplementary information (ESI) available. CCDC 1497307 and 1497308. For ESI and crystallographic data in CIF or other electronic format see DOI: 10.1039/c6dt03769k

The nitrate-intercalated LDH offers additional possibilities. Among the more widely studied II–III LDHs, the NO_3^- ion is known to intercalate with its molecular plane inclined at an angle to the metal hydroxide layer at a high layer charge.[8–10] At low values of layer charge, it intercalates with its molecular plane parallel to the metal hydroxide layer. Besserguenev and coworkers[6] have shown that in the dehydrated phase of the [Li–Al–NO_3] LDH, the nitrate ion is intercalated with its molecular plane parallel to the metal hydroxide layer. Consequently the basal spacing is 7.2 Å which corresponds to a one-atom thick interlayer. The hydrated [Li–Al–NO_3] LDH, on the other hand has a basal spacing of 8.9 Å.[5] The variation in the basal spacing with hydration makes this structural transition interesting. However, no structure model has yet been proposed for the hydrated phase of the [Li–Al–NO_3] LDH.

The Li–Al LDHs are unique as they exhibit shape selective anion exchange reactions.[11,12] Further, among all the inorganic anions, the NO_3^- ion is the most labile leaving group, making the NO_3^- intercalated LDH the most favoured precursor for all the exchange reactions.[13] It is therefore important to understand the packing of atoms in the interlayer galleries of the hydrated and dehydrated phases of the [Li–Al–NO_3] LDH. This article is an effort in this direction.

Experimental

Gibbsite was provided by the Jawaharlal Nehru Aluminum Research Development and Design Center (Nagpur, India). The [Li–Al–NO_3] LDH was prepared by imbibition of $LiNO_3$ into gibbsite. 0.5 g of gibbsite was soaked in 10 mL of ~10 M $LiNO_3$ solution and hydrothermally treated in a Teflon-lined autoclave (80 mL capacity) at 140 °C (24 h). The sample was centrifuged, washed with Type II water (specific resistance 15 MΩ cm, Millipore Academic water purification system) and dried in a hot air oven at 65 °C.

Wet chemical analysis

The Li content was estimated using flame photometry and the NO_3^- ion content using ion chromatography (Metrohm Model 861 Advanced Compact Ion Chromatograph with Metrosep SUP5 150 column). The intercalated water content was determined by thermogravimetry (Mettler Toledo TG/SDTA Model 851^e system, 30–900 °C, heating rate 5 °C min^{-1}, flowing air). The IR spectra of the samples were recorded using the Bruker model Alpha-P IR spectrometer (Diamond ATR cell, 4 cm^{-1} resolution, 400–4000 cm^{-1}).

Characterization

The sample was characterized by powder X-ray diffraction (PXRD) (Bruker D8 Advance diffractometer, Cu Kα radiation, λ = 1.5418 Å) operated in reflection geometry. Data were collected at a continuous scan rate of 1° 2θ min^{-1} and a step size of 0.02° 2θ. For the structure refinement of the as prepared (phase-I) LDH, data were recorded over a 5–100° 2θ range (step size of 0.02° 2θ, counting time 10 s per step). To confirm the reversible hydration behaviour of the LDH, variable temperature PXRD data were recorded using a variable temperature cell Model A18-A100 with a Ta strip heater. For the structure refinement of the dehydrated (phase-II) LDH, *in situ* data were obtained using an Empyrean powder X-ray diffractometer equipped with a Cu Kα source, λ = 1.5418 Å, and a high-temperature vacuum Anton Paar camera TK1200 (Moscow State University, Russia). Unit cell parameters were obtained from POWDER and refined using APPLEMAN, part of the PROSZKI suite of programs. The interlayer structure of phase-I was obtained using the code FOX. The structure refinement of phase-II was carried out in code GSAS. For the refinement, a TCH-pseudo-Voigt line shape function (Profile Function 2) with eight variables was used to fit the experimental profile. The shifted Chebyshev polynomial function with 24 terms is used to correct the background.

Computational method

All structures were optimized by DFT methods using the SIESTA package,[14] which consists of localized molecular orbital basis sets. All atoms are represented with Troullier–Martins norm conserving pseudo potentials in the Kleinman–Bylander form together with the gradient corrected Perdew, Burke, and Ernzerhof (PBE) exchange correlational functional.[15] A double-z basis (DZP)[16] set with the polarization orbitals is included for all atoms together with a real-space mesh cut-off of 300 Ry. The Grimme-D3 [17] dispersion correction has been included to describe the long-range interaction. During geometry optimization, no symmetry constraints of any kind were imposed and interatomic forces were relaxed up to 0.01 eV $Å^{-1}$. The cell size was stabilized for the calculations by corroborating the computed with the reported structural parameters[6] for validation. A good match of the computed and experimental structural parameters was obtained for the cell size $2a \times \sqrt{3}a \times c$ (10.3 × 8.9 × 14.4 $Å^3$). This is four times the volume of the hexagonal unit cell. All other structures were optimized using the same cell size. The total energies were calculated at the gamma point.

Results and discussion

The as-prepared [Li–Al–NO_3] LDH (phase-I) has a PXRD pattern dominated by two basal reflections which appear at 8.92 Å (9.92° 2θ) and 4.46 Å (19.97° 2θ) respectively. Thermogravimetric analysis of phase-I (Fig. S1†) shows that about 10% of mass is lost at 175 °C. Combining these results with those of flame photometry (Li content) and ion chromatography (NO_3^- content) yields an approximate chemical formula $[LiAl_2(OH)_6]$ $(NO_3)\cdot 1.2H_2O$ for phase-I. On heating phase-I, there is an abrupt change in the PXRD pattern at 50 °C *in vacuo*. The basal reflections shift to higher angles at 7.2 Å (12.3° 2θ) and 3.6 Å (24.6° 2θ) (Fig. S2†). Basal spacing contraction is accompanied by a dramatic increase in the relative intensities of all non-00l reflections. Thereafter the positions of reflections remain unaltered on further heating until

200 °C (Fig. S3†) above which decomposition sets in. The PXRD pattern recorded at 175 °C matches closely with that reported by Besserguenev and coworkers,[6] at 175 °C for the fully dehydrated phase. The basal spacing contracts even before the dehydration is complete. In keeping with previous observations, the dehydrated phase (referred as phase-II) is hygroscopic and rapidly undergoes rehydration.

A close look at the PXRD pattern of phase-I on an expanded intensity scale reveals several weak reflections in the range of 11–19° 2θ and 22–35° 2θ (Fig. 1). While all the major reflections, in keeping with suggestions from earlier work,[6] could be indexed to a hexagonal cell (a_o = 5.087 Å; c_o = 17.909 Å) (Table S1†), the weak reflections could not be indexed. The question arose whether these reflections were due to impurities. Likely impurities in this system are $LiAlO_2$ and single cation phases such as Al_2O_3, AlO(OH), Li_2O, and LiOH. None of these candidate impurities could account for these weak reflections. However these weak reflections are completely extinguished on heating (Fig. 1b). On cooling and rehydration, the weak reflections reappear (Fig. 1c) suggesting that this set of weak reflections are not only intrinsic to phase-I, but are also associated with the massive reorganization in the packing of atoms in the interlayer galleries during hydration. These additional reflections could arise either from (i) a trigonal/hexagonal cell of large volume or (ii) from a cell of lower symmetry.

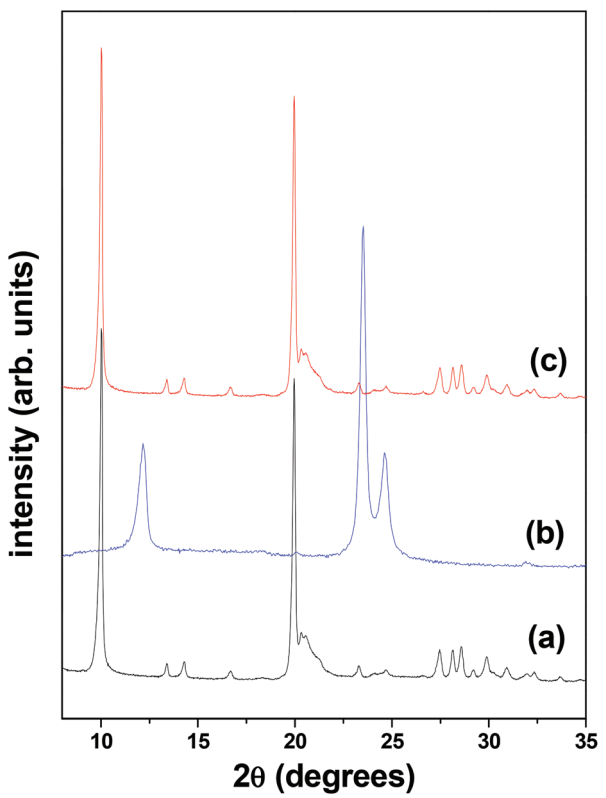

Fig. 1 PXRD pattern of the gibbsite-derived [Li–Al–NO_3] LDH: (a) hydrated, (b) dehydrated at 50 °C *in vacuo*, and (c) (b) rehydrated under ambient conditions on standing.

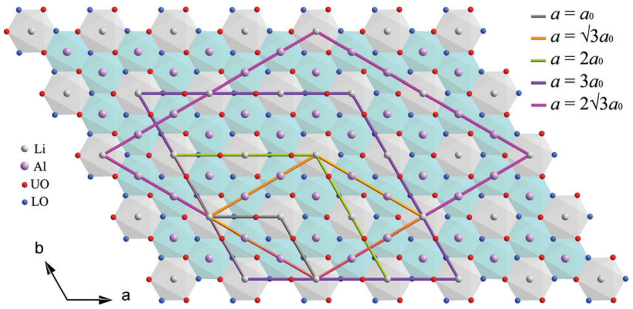

Fig. 2 The structure of the $[LiAl_2(OH)_6]^+$ layer showing different possible supercells of hexagonal symmetry.

In the first instance, four supercells of hexagonal symmetry were considered (Fig. 2): (i) $a = b = \sqrt{3} \times a_o$, (ii) $a = b = 2 \times a_o$, (iii) $a = b = 3 \times a_o$, and (iv) $a = b = 2\sqrt{3} \times a_o$ (a_o = 5.087 Å). Later even larger unit cells up to $a = b = 7 \times a_o$ were considered. The Bragg reflections corresponding to each of these supercells were generated and compared with the observed weak reflections (see Table 1 as illustration). None of the supercells generate all the observed weak reflections, thereby showing that it is unnecessary to select a cell of higher volume.

Closely related to the [Li–Al] LDHs are the Li-oxides of the general formula $LiMO_2$ (M = Ni^{3+}, Co^{3+}, Mn^{3+}).[18,19] These oxides are structurally the inverse of the LDHs, comprising as they do, a stacking of negatively charged layers of the composition $[MO_2]^-$, with the Li^+ ions intercalated in the interlayer galleries. They crystallize in either rhombohedral or hexagonal crystal symmetry very similar to the LDHs. Often the transition metal oxide layer comprises two different cations, such as for instance $[Ni_{1-x}Mn_xO_2]^-$. While all the major reflections of this oxide could be indexed to the well-known rhombohedral polytype (space group $R\bar{3}m$, a_o = 2.88 Å), numerous weak reflections similar to those reported here, were observed in the range of

Table 1 Indexing of weak reflections with the supercells of hexagonal symmetry

	$a = a_o$ 5.08 Å	$a = \sqrt{3} \times a_o$ 8.81 Å	$a = 2 \times a_o$ 10.17 Å	$a = 3 \times a_o$ 15.27 Å	$a = 2\sqrt{3} \times a_o$ 17.52 Å
2θ [°]	*hkl*	*hkl*	*hkl*	*hkl*	*hkl*
13.3	—	—	—	—	—
14.2	—	—	—	—	112
16.6	—	—	—	—	—
23.2	—	—	—	—	204
24.0	—	—	—	204	—
24.6	—	—	—	—	—
27.4	—	—	—	401	411
28.1	—	—	—	—	—
28.5	—	—	212	313	224
29.1	—	—	—	—	314
29.8	—	—	—	321	501
30.8	—	204	301	224	—
31.9	—	—	—	—	—
32.3	—	—	205	116	206
34.7	—	—	—	—	423

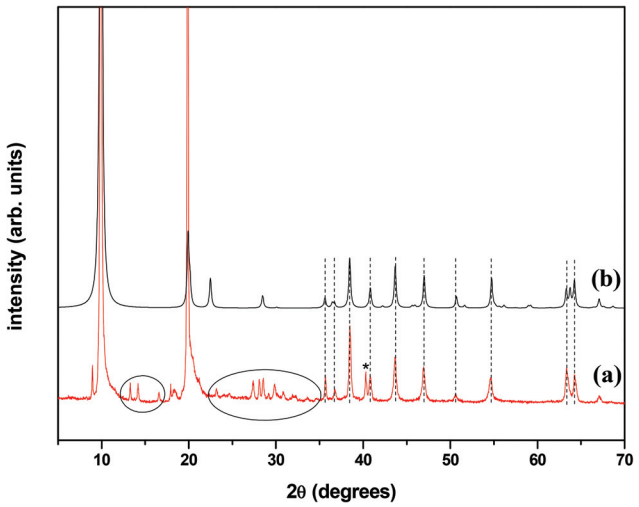

Fig. 3 (a) The observed PXRD pattern of the as-prepared [Li–Al–NO_3] LDH compared with (b) the DIFFaX simulated pattern for the PP̄P··· stacking of the [Li–Al] metal hydroxide layer. The peak marked with an asterisk in the experimental pattern is due to the basal reflection 008.

20–30° 2θ. These could not be indexed to a three-layer rhombohedral cell. In this case the authors selected a cation ordered unit mesh $a_o \times \sqrt{3}a_o$ and constructed a one-layer cell of monoclinic symmetry (β = 109°). All the observed weak reflections could then be indexed. All the reflections earlier indexed to the rhombohedral cell could also be indexed to the one-layer monoclinic cell.

We therefore attempted a similar strategy. The key to the successful choice of a monoclinic cell is to find the appropriate value for the stacking angle β, in *c*-stacking.[20] In this we were greatly aided by DIFFaX simulations (Fig. 3). The metal hydroxide layer was taken from the structure of the [Li–Al–Br] LDH refined earlier.[7] We designate such a layer by the symbol P. The mirror image of this layer is given the symbol P̄. As the [Li–Al–NO_3] LDH reported here is obtained from the gibbsite precursor (space group $P12_1/n1$), the interlayer relationship of the precursor is likely to be conserved in the LDH crystal. Gibbsite is a two layer cell of monoclinic symmetry comprising PP̄P··· stacking. A simulation of the PP̄P··· stacking of the [Li–Al] metal hydroxide layer generates all the observed major reflections for the stacking angle 90°. When the stacking angle was varied by imparting relative translations of *a*/2, *a*/3, *a*/4, *etc.* between the adjacent layers, the major reflections appearing in the 35°–60° 2θ region went out of registry with the observed reflections and did not regain registry over the entire range of stacking angles (95°–106°) thereby eliminating the possibility of monoclinic symmetry. A β value of 90° suggests a cell of orthorhombic symmetry, with a *c*-parameter (17.86 Å) twice the basal spacing.

To index the whole pattern, including all the weak reflections, code POWDER from the PROZSKI suite of programmes was used, without the imposition of any symmetry restraints using the default limiting cell volume of 1000 Å^3. Several solutions were generated none of which had any of the cell edges close to the expected *c*-parameter of 17.86 Å. Special emphasis was also laid on the relationship of any one cell edge, say *c*, with any one angle, say β to verify the relationship that the first basal spacing = $c \sin\beta$ or $\frac{1}{2} c \sin\beta$, which should be satisfied for monoclinic symmetry without success. The limiting cell volume was progressively increased to generate even more possible solutions.

Eventually an orthorhombic cell *a* = 12.50 Å, *b* = 15.72 Å, and *c* = 17.88 Å was found which could index all the observed reflections. This solution reinforced the results of the DIFFaX simulations (Fig. 3) which predict β = 90°. All the reflections indexed earlier to the hexagonal cell were also indexed to the orthorhombic cell (Table 2). While there is a perfect match of the *c*-parameters, there is no relationship between the *a* and *b* parameters of the hexagonal and orthorhombic unit cells, suggesting that phase-I probably crystallizes in an incommensurate structure.

To conclude this section, the results described hitherto can be summarized as follows.

(i) The as prepared [Li–Al–NO_3] LDH (phase-I) is a single phase material.

(ii) The powder X-ray diffraction pattern comprises two sets of reflections: one set of intense reflections is due to a hexa-

Table 2 Observed Bragg reflections in the PXRD pattern of the as-prepared [Li–Al–NO_3] LDH (phase-I) indexed to the cells of hexagonal and orthorhombic symmetry

	Hexagonal *a* = 5.087 Å, *c* = 17.909 Å	Orthorhombic *a* = 12.502 Å, *b* = 15.726 Å, *c* = 17.877 Å
2θ [°]	*hkl*	*hkl*
9.9	002	002
13.3	—	120
14.2	—	200
16.6	—	122
19.9	004	004
23.2	—	041
24.0	—	124
24.6	—	321
27.4	—	025
28.1	—	143
28.5	—	400
29.1	—	332
29.8	—	314
30.8	—	420
31.9	—	250
32.3	—	251
34.7	—	145
35.7	111	154
36.8	112	511
38.5	113	217
40.3	008	531
40.8	114	170
43.6	115	173
46.9	116	630
50.6	117	642
54.6	118	059
63.4	300	754
64.2	302	824
67.1	217	708
73.5	304	1612

gonal cell and the other set of weak reflections is due to a cell of orthorhombic symmetry.

(iii) In keeping with similar observations in other systems,[14,15] phase-I could be treated as a solid solution of two different lattices.

Structure refinement

In the next stage, structure refinement was taken up. The refinement of the structure of the phase-II was taken up first as (i) it is uncomplicated by the appearance of weak reflections, (ii) the corresponding dehydrated structure with matching basal spacing (c = 7.2 Å) has been investigated by earlier authors,[6] on account of which a structure model is readily available, and (iii) the metal hydroxide layer is expected to be invariant during the dehydration process.

The Le Bail fit of the PXRD pattern of phase-II was performed using code GSAS in the space group $P6_3/mcm$. The shifted Chebyshev function with 24 terms was used to fit the background. The goodness of fit parameters for the fit were R_{wp} = 0.0676, R_p = 0.0532, and χ^2 = 3.588. The c-parameter at 14.44 Å indicates a two layer cell, where the adjacent layers are related by a mirror plane reflection. The Rietveld procedure was initiated with the introduction of a partial structure model consisting of only the metal hydroxide layer. All the profile and cell parameters were refined. The computed difference Fourier indicates electron densities at 2a (0, 0, 0.25), 6g (0.48, 0, 0.25) and 12j (0.33, 0.14, 0.25) sites with the ρ values of 14.97, 5.8, and 4.15 respectively in the interlayer midway between the adjacent metal hydroxide layers. The N atom was introduced at the 2a site, and O atoms in the two other positions. The structural parameters of the newly added atoms were individually refined, followed by the structural parameters of the atoms in the metal hydroxide layer. The 004 reflection was over estimated, which was corrected by the introduction of preferred orientation along 002. At this stage R_{wp} = 0.1202, R_p = 0.0904, χ^2 = 8.967, and $R(F^2)$ = 0.1008 were realized. The difference Fourier computed at this point did not indicate any significant electron density. The final Rietveld fit (Fig. 4) is satisfactory. The details of the refinement, structural parameters and the bond distance and angles are given in Tables 3–5.

A plot of the structure (Fig. 5) shows that the molecular plane of the NO_3^- ion is parallel to the metal hydroxide layer. There is disorder in the position of the O atoms of the nitrate ion. O atoms in excess of those associated with the NO_3^- ion had to be included to meaningfully account for the electron density in the interlayer. We believe that the structure is not fully dehydrated and there is residual intercalated water which is strongly bonded to the sample and not released on heating *in vacuo* at 50 °C. This probably accounts for the choice of the $P6_3/mcm$ space group in this work, compared to $P6_3/m$ chosen in the earlier work.[6] Nevertheless, to validate the choice of the $P6_3/mcm$ space group, Rietveld refinement of the structure was also carried out in the $P6_3/m$ space group. The resultant R values were higher than those reported here.

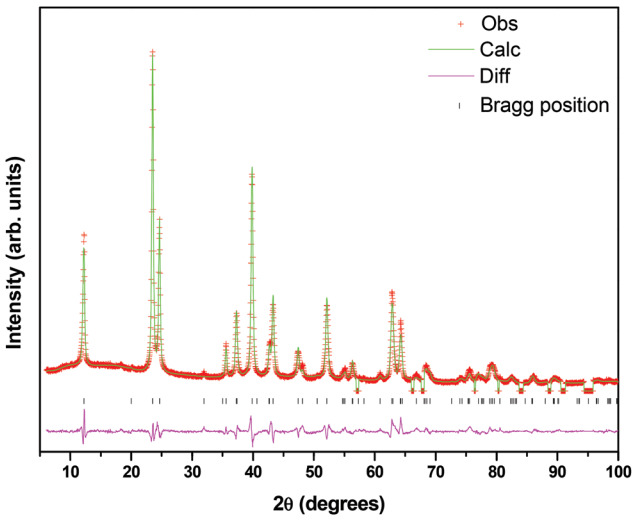

Fig. 4 A Rietveld fit of the PXRD pattern of the dehydrated [Li–Al–NO_3] LDH (phase-II).

Table 3 Results of Rietveld refinement of the structure of the dehydrated and hydrated [Li–Al–NO_3] LDHs

	Phase-I	Phase-II
Crystal system	Hexagonal	Hexagonal
Space group	$P6_3/m$	$P6_3/mcm$
Cell parameters [Å]	a = 5.0835(4), c = 17.8691(4)	a = 5.12524(13), c = 14.4462(6)
Volume [Å^3]	399.90(4)	328.634(19)
Data points	4751	2683
Parameters refined	52	49
R_{wp}	0.225 (0.1967)[a]	0.0825
R_p	0.164 (0.1028)[a]	0.0675
$R(F^2)/R_F$	0.0829 [R_F]	0.0666 [$R(F^2)$]
χ^2	6.357	5.836
R_{Bragg}	0.0637	—

[a] Values given in parenthesis are obtained from code FOX.

Structure refinement of phase-I

A Rietveld fit of the PXRD pattern of phase-I was attempted excluding all the minor reflections which could not be indexed to a hexagonal cell. A Le Bail fit was performed in the space group $P6_3/m$ using code FOX (R_{wp} = 0.1471, R_p = 0.1080). At this stage, the metal hydroxide layer obtained from phase-II was introduced into the refinement procedure as a partial structure model. Within the FOX formalism, the nitrate ion and the water molecule were introduced into the interlayer gallery as molecular units. The observed values of the N–O bond length and the O–N–O bond angle were chosen as the initial guess. The nitrate ion and the O atom of the intercalated water were allowed to translate randomly in the interlayer gallery. After each translation, the nitrate ion was rotated. The N–O bond lengths and O–N–O bond angles were allowed to vary with default constraints embedded in the code. For securing a stable refinement, the N atom of the intercalated nitrate ion was restricted to a plane midway into the interlayer gallery

Table 4 Refined atomic position parameters of dehydrated [Li–Al–NO_3] LDH (phase-II)

Atom type	Wyckoff position	x	y	z	Occupancy	U_{iso}
Li	2b	0	0	0	1.0	0.03104
Al	4d	0.3333	0.6667	0	1.0	0.00769
O1	12k	0.65058	0.65058	0.57229	1.0	0.01015
N	2a	0	0	0.25	1.0	0.0269
O2	12j	0.205	−0.08656	0.25	0.5	0.07597
Ow	6g	0.57698	0	0.25	0.316	0.1

Table 5 Refined bond lengths and bond angles of [Li–Al–NO_3] LDH (phase-II)

Bond lengths [Å]	
Al–O1	1.96831(4), 1.96851(4), 1.96874(4)
Li–O1	2.07309(4)
N–O2	1.32923(3)
N–Ow	2.16809(5)
Bond angles [°]	
O1–Li–O1	83.1425(16), 96.8575(16)
O1–Al–O1	82.5312(18), 82.5482(18), 88.6557(16), 88.6738(16), 94.4606(17), 94.4669(17), 94.4742(17)

(z = 0.25). A Monte Carlo procedure was used with the various R values as the cost function. This refinement procedure carried out in direct space yielded a chemically appropriate structure model (R_{wp} = 0.1967, R_p = 0.1028). This model structure was imported to the FULLPROF suite to complete the refinement (Fig. 6 and Table 3) in a conventional way within the reciprocal space. The poor value of R_{wp} is on account of the excluded region, which makes the background refinement relatively inaccurate. The R_F and R_{Bragg} values (FULLPROF) are within the acceptable range. The R_p value, which actually estimates the point by point error is acceptable in the evaluation by code FOX, but higher in code FULLPROF, although the visual quality of the fit and the structural parameters do not significantly differ in the two codes. The overall balance of judgement tilts in favour of the proposed structure model to the limited extent that it establishes (i) the symmetry of the metal hydroxide sublattice and (ii) accounts for the expansion of the basal spacing due to the reorientation of the nitrate ion. The resulting structure (Fig. 7) shows that the nitrate ion is inclined to the metal hydroxide layer at an angle ~48° and accounts for the expansion of the c-parameter on hydration. The position parameters, bond lengths and bond angles (Tables S2 and S3†) extracted from the refined structure are reasonable.

As the complete PXRD pattern of phase-I was indexed to an orthorhombic cell, we proceeded to the next step to identify the possible space group. In this we were guided initially by the *translationengleiche* subgroups of the $P6_3/mcm$ summit, assuming the high symmetry phase-II, to be the parent symmetry for this class of compounds. The partial structure of

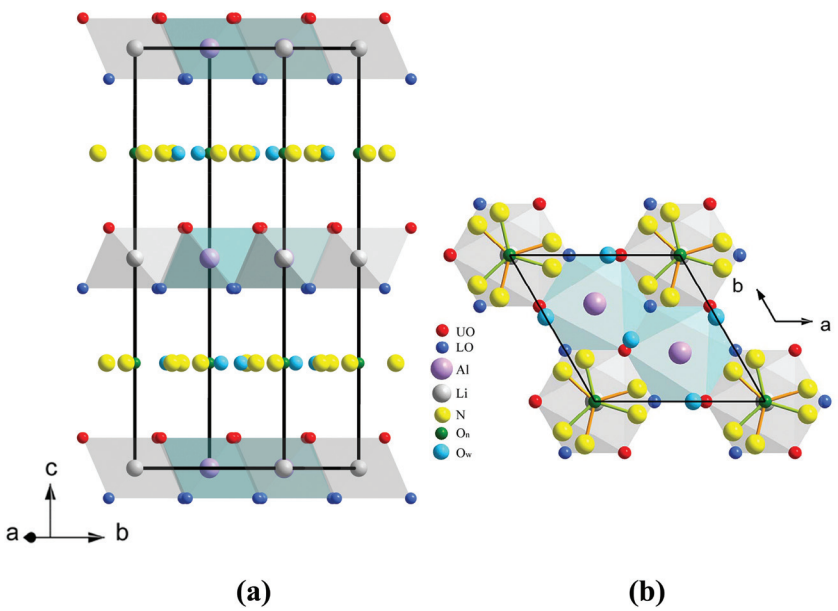

Fig. 5 (a) The refined structure of phase-II [Li–Al–NO_3] viewed along 100. (b) One [$LiAl_2(OH)_6$] layer and the adjacent interlayer viewed down the c-axis. UO and LO are respectively the upper and lower hydroxyl oxygen atoms of the metal hydroxide layer. O_n is the oxygen atom of the intercalated nitrate ion and O_w is the oxygen atom of the intercalated water molecule.

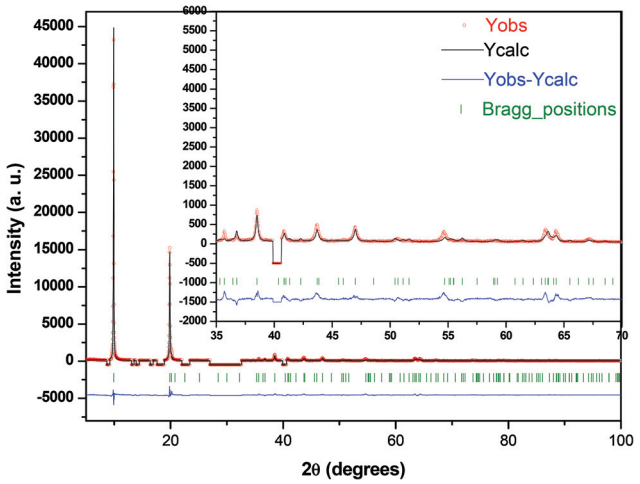

Fig. 6 A Rietveld fit of the observed PXRD profile of phase-I with the minor reflections excluded. In the inset is an expansion of the fit in the 2θ range 30–70°.

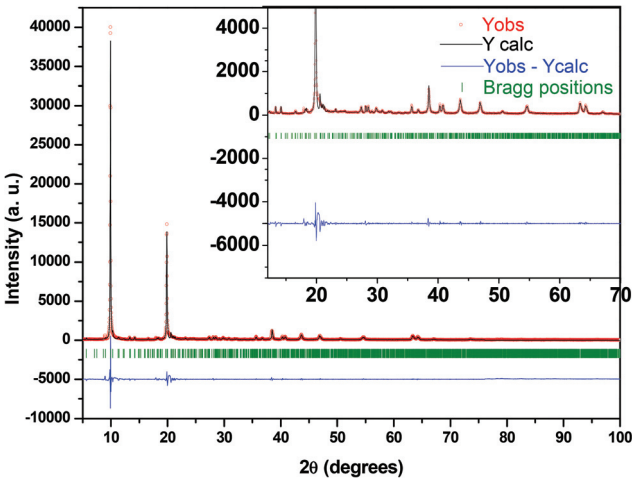

Fig. 8 Le Bail fit of the PXRD pattern of phase-I in orthorhombic symmetry (*P*222).

phase-I, $P6_3/m$ is a prominent subgroup of $P6_3/mcm$. This summit generates only one subgroup of orthorhombic symmetry, *Cmcm*.

A Le Bail fit of the complete pattern of phase-I was attempted using the space group *Cmcm* and its related orthorhombic subgroups of lower symmetry. None of these space groups could generate all the observed reflections. All the reflections could be generated, only when no reflection conditions were imposed. The candidate space groups are *P*222, *Pmm*2 and *Pmmm* of which *P*222 was chosen rather arbitrarily (Fig. 8, R_{wp} = 0.1607, R_p = 0.1027). The Rietveld fit of the complete profile could not be carried out due to the non-availability of a structure model.

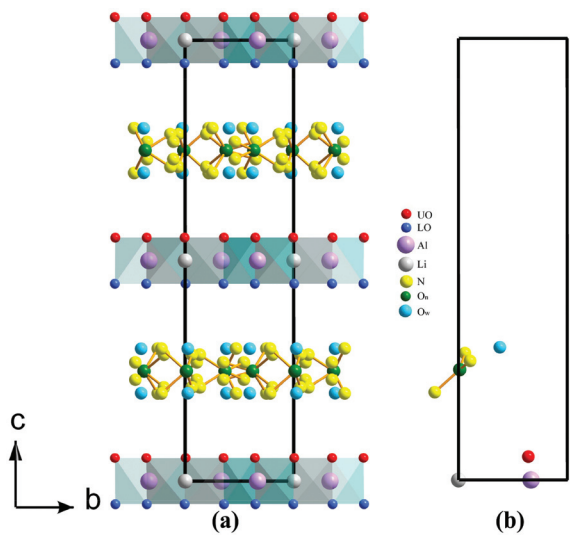

Fig. 7 The complete unit cell (left panel) and the symmetry distinct atoms showing the plane of the nitrate ions inclined to the metal hydroxide layer (right panel) in the crystal of phase-I.

To conclude, the dehydrated phase includes the nitrate ion with its molecular plane parallel to the metal hydroxide layer (coordination symmetry D_{3h}). On hydration, the nitrate ion reorients itself so that its molecular plane is inclined to the metal hydroxide layer (coordination symmetry C_s).

DFT computations

To understand the hydration behaviour, DFT computations were carried out on the hydration of phase-II. In the first instance, the refined structure of phase-II (dehydrated) was input into code SIESTA and relaxed without the imposition of any constraints. The structure did not depart significantly from the initial input as evident from the computed cell parameters (Table 6). The computed basal spacing is 7 Å which is in agreement with that of phase-II. The position and orientation of the nitrate ion also did not depart from the initial choice.

To understand the phenomenon of hydration, water molecules were introduced into the interlayer. Initially the water molecules were inserted in the same plane as that of the nitrate ions. A total of 16 water molecules were included in the supercell used for the computation, to account for the experimentally determined composition. Considering the van der Waals diameter of water (2.8 Å) and the $NO_3^-\cdots NO_3^-$ distance in the interlayer, the number density of atoms in the interlayer is too large to be realistic. An expansion of the basal spacing accompanied by the reorientation to the nitrate ion is expected. Even though no constraints were imposed, computations did not result in the expansion of the basal spacing which remained at 7.1 Å even after 500 iterations, and the energy did not converge. Enormous force was developed in the *a*–*b* plane (Table 7), but the force along the *c*-axis was close to zero, explaining the inability of the structure to expand the basal spacing. The large in plane force resulted in the expansion of the unit mesh in the interlayer compared to the metal hydroxide layer (Fig. 9). The resulting phase would then be a

Table 6 Comparison of experimental and computed cell parameters of the dehydrated and hydrated [Li–Al–NO_3] LDH

	Dehydrated		Hydrated		
				Computed	
	Experimental[a]	Computed	Experimental[a]	Flat	Tilt
a (Å)	10.2504	10.3742	10.1670	10.7765	10.5242
b (Å)	8.8771	8.9811	8.8049	10.9247	8.9131
c (Å)	14.4462	13.8723	17.8691	15.0965	18.3949
α (°)	90	90.005	90	89.996	92.007
β (°)	90	89.996	90	89.999	91.67
γ (°)	90	90.002	90	90.466	88.479

[a] Cell parameters are of the supercell used for computation.

"solid solution" of two lattices: (i) the hexagonal lattice of the metal hydroxide layer, and (ii) the lattice defining the spacing of the interlayer moieties, the two lattices being out of registry with one another. In order to generate force parallel to the c-axis, the optimization was repeated by adding water molecules in a bilayer above and below the layer of the intercalated nitrate ions. On computing without the imposition of any restraints, the nitrates were found to rotate and adopt a configuration in which their molecular plane was inclined at angles in the range 56–71° ('tilt' in Table 7) with the metal hydroxide layer. Together with this the basal spacing expanded to 9.1 Å, close to the experimental value of the as-prepared phase. The experimental and the computational results offer two limiting models for the behaviour of LDHs on hydration.

(i) In the first model, the stacking of the metal hydroxide layers remain rigid and hydration generates in-plane repulsive forces which destroys the registry in the ordering of the intercalated species with the periodicity of the metal hydroxide layer.

(ii) In the second model, hydration of the interlayer moieties increases indefinitely, with concomitant expansion of the basal spacing leading eventually to delamination.

Table 7 RMS[a] value of forces exerted by atoms in the interlayer along the three crystallographic axes in the computed structures

Units (eV Å^{-1})	a	b	c
Dehydrated	0.010398	0.008704	0.000165
Hydrated-flat[b]	0.694851	0.663705	0.000326
Hydrated-tilt	0.001610	0.001932	0.001856

[a] The forces mentioned in the table are the root of the mean square of the sum of forces exerted by all the atoms in the interlayer. [b] After 500 iterations.

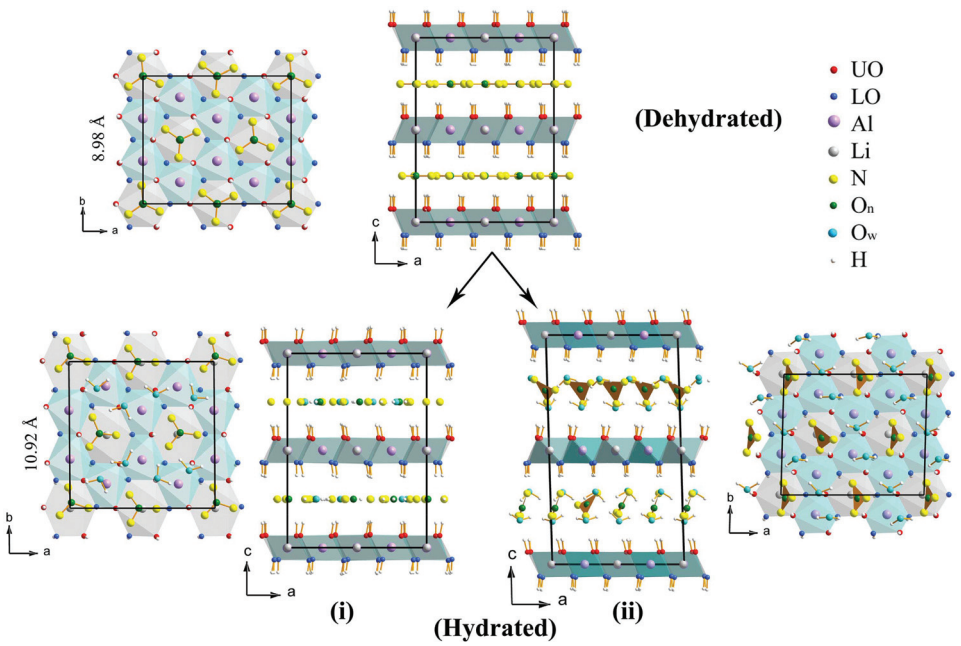

Fig. 9 Computed structure of the dehydrated LDH and the results of hydration: (i) shows an in-plane expansion of the nitrate sublattice without any expansion of the basal spacing, (ii) shows the expansion of the basal spacing without any change in the unit mesh of the intercalated layer.

The observed behaviour of the LDH is in between the two possible limiting models, involving a moderate expansion of the basal spacing as well as the generation of a unit mesh 12.5 Å × 15.7 Å, which is larger than that of the metal hydroxide layer.

Conclusions

Introduction of water in the interlayer galleries of the nitrate-intercalated LDH results in a massive reorganization in the arrangement of the nitrate ions. The resulting sublattice has neither the hexagonal symmetry of the metal hydroxide layers, nor the monoclinic symmetry derived by distortion in the hexagonal stacking. On the other hand, the interlayer atoms are indexed to a cell of orthorhombic symmetry. This kind of arrangement of atoms in the interlayer is on account of the interplay between competing forces that expand the crystal in the *a*–*b* plane and those that expand the crystal along the *c*-axis.

Acknowledgements

The authors thank Professor V. V. Chernyshev of the M. V. Lomonosov Moscow State University, Russia for many useful discussions. The authors also thank the Department of Science and Technology (DST), Government of India (GOI) for financial support. SN is a recipient of a Senior Research Fellowship (NET) of the University Grants Commission, India. PVK is a recipient of the Ramanna Fellowship of the DST, GOI.

References

1 K. R. Poeppelmeier and S.-J. Hwu, *Inorg. Chem.*, 1987, **26**, 3297–3302.
2 A. F. Wells, *Structural Inorganic Chemistry*, English Language Book Society and Oxford University Press, 4th edn, 1975.
3 C. J. Serna, J. L. Rendon and J. E. Iglesias, *Clays Clay Miner.*, 1982, **30**, 180–184.
4 J. P. Thiel, C. K. Chiang and K. R. Poeppelmeier, *Chem. Mater.*, 1993, **5**, 297–304.
5 X. Hou, D. L. Bish, S. L. Wang, C. T. Johnston and R. J. Kirkpatrick, *Am. Mineral.*, 2003, **88**, 167–179.
6 A. V. Besserguenev, A. M. Fogg, R. J. Francis, S. J. Price and D. O'Hare, *Chem. Mater.*, 1997, **2**, 241–247.
7 S. Nagendran and P. V. Kamath, *Eur. J. Inorg. Chem.*, 2013, **2013**, 4686–4693.
8 S. L. Wang and P. C. Wang, *Colloids Surf., A*, 2007, **292**, 131–138.
9 M. Jobbágy and N. Iyi, *J. Phys. Chem. C*, 2010, **114**, 18153–18158.
10 S. Marappa, S. Radha and P. V. Kamath, *Eur. J. Inorg. Chem.*, 2013, 2122–2128.
11 A. M. Fogg, V. M. Green, H. G. Harvey and D. O'Hare, *Adv. Mater.*, 1999, **11**, 1466–1469.
12 S. W. Rhee, J. H. Lee and D.-Y. Jung, *J. Colloid Interface Sci.*, 2002, **245**, 349–355.
13 A. I. Khan, A. Ragavan, B. Fong, C. Markland, M. O'Brien, T. G. Dunbar, G. R. Williams and D. O'Hare, *Ind. Eng. Chem. Res.*, 2009, **48**, 10196–10205.
14 J. M. Soler, E. Artacho, J. D. Gale, A. Garcìa, J. Junquera, P. Ordejòn and D. Sànchez-Portal, *J. Phys.: Condens. Matter*, 2002, **14**, 2745–2779.
15 J. P. Perdew, K. Burke and M. Ernzerhof, *Phys. Rev. Lett.*, 1996, **77**, 3865–3868.
16 O. F. Sankey and D. J. Niklewski, *Phys. Rev. B: Condens. Matter*, 1989, **40**, 3979–3995.
17 S. Grimme, J. Antony, S. Ehrlich and H. Krieg, *J. Chem. Phys.*, 2010, **132**, 154104.
18 K. A. Jarvis, Z. Deng, L. F. Allard, A. Manthiram and P. J. Ferreira, *Chem. Mater.*, 2011, **23**, 3614–3621.
19 K. A. Jarvis, Z. Deng, L. F. Allard, A. Manthiram and P. J. Ferreira, *J. Mater. Chem.*, 2012, **22**, 11550–11555.
20 K. Jayanthi, S. Nagendran and P. V. Kamath, *Inorg. Chem.*, 2015, **54**, 8388–8395.